Applied Catalysis B: Environmental 170-171 (2015) 215–224

Contents lists available at ScienceDirect

Applied Catalysis B: Environmental

journal homepage: www.elsevier.com/locate/apcatb

Effect of surface modification with H_2S and NH_3 on TiO_2 for adsorption and photocatalytic degradation of gaseous toluene

Fan Zhang[a], Mengjiao Wang[b], Xiaodi Zhu[a], Bin Hong[a], Wendong Wang[c], Zeming Qi[a], Wei Xie[a], Jianjun Ding[a,b], Jun Bao[a,b], Song Sun[a,b,*], Chen Gao[a,b,**]

[a] National Synchrotron Radiation Laboratory, Collaborative Innovation Center of Chemistry for Energy Materials, University of Science & Technology of China, Hefei, Anhui 230029, China
[b] CAS Key Laboratory of Materials for Energy Conversion, Department of Materials Science and Engineering, University of Science & Technology of China, Hefei, Anhui 230026, China
[c] Department of Chemical Physics, University of Science & Technology of China, Hefei, Anhui 230026, China

ARTICLE INFO

Article history:
Received 11 December 2014
Received in revised form 28 January 2015
Accepted 31 January 2015
Available online 2 February 2015

Keywords:
Surface Modification
TiO_2
Photocatalysis
Toluene
In situ DRIFTS

ABSTRACT

This study investigates the effects of surface modification with H_2S and NH_3 respectively on the photocatalytic activity of TiO_2 for toluene degradation. Surface modification with H_2S was observed to enhance the adsorption of toluene and promote the degradation rate at the start of photocatalytic degradation, while that with NH_3 inhibited the adsorption of toluene but enhanced the photocatalytic activity for the toluene degradation. By a combination of in situ DRIFTS and other characterization methods, the adsorption mechanism and relationship between surface structure and photocatalytic activity were proposed. For TiO_2–H_2S, the sulfhydryl group, which is formed from the dissociation of H_2S molecules, could easily interact with toluene. The low photocatalytic activity may be caused by the inhibition of the regeneration of surface hydroxyl groups, poor generation of $O_2^{-\bullet}$ radicals and accumulation of highly stable intermediates. For TiO_2–NH_3, steric hindrance serves as interference to the adsorption of toluene, while the abundant surface hydroxyl groups are possibly conducive to the degradation of toluene.

1. Introduction

Toluene is one of the typical volatile organic compounds (VOCs) in the indoor environment, which is emitted from decoration materials, paint, and cementing compounds. In recent years, extensive research related to the removal of toluene has been reported [1–4], and heterogeneous photocatalytic oxidation (PCO) has been considered to be an attractive method for the degradation of toluene, as it can treat pollutants under mild operating conditions [5–8]. Currently, TiO_2 is the most widely used photocatalyst for the degradation of toluene because of its stability, low cost, innocuousness, and relatively high activity [9,10]. To date, the majority of mechanistic studies on the photocatalytic degradation of toluene on TiO_2-based surfaces involves the adsorption sites and structure, reaction intermediates, and kinetics [11–15].

Effective adsorption is the first key step for photocatalytic degradation [16,17]. Maira and Soria's group [18,19] found that there are two types of hydroxyl groups on the TiO_2 surface: isolated hydroxyls and H-bonded hydroxyls. It was speculated that weak bonding exists through the OH···π-electron-type interaction between the surface hydroxyl groups and the aromatic ring of toluene adsorbed on TiO_2 [20,21]. In our previous study, based on in situ far infrared spectroscopy and theoretical simulations, this specific adsorption of toluene on the TiO_2 surface was hypothesized to entail three possible adsorption structures: ortho-, meta-, and para-adsorption structures [22]. It should be pointed out that the adsorption sites of TiO_2 are not limited to hydroxyl groups. The coordinatively unsaturated surface Ti^{n+} and oxygen vacancies are also considered as active centers for toluene adsorption [23,24], which complicates the surface adsorption of TiO_2. For the photocatalytic process, some studies indicated that the surface hydroxyl groups of TiO_2 play an important role in the photocatalytic oxidation of toluene as they can directly participate in the oxidation reaction by trapping the charge carriers reaching the photocatalyst surface to produce very reactive surface $OH^{\bullet}$ radicals [25,26] which were suggested to be

* Corresponding author at: University of Science and Technology of China, National Synchrotron Radiation Laboratory, Hezuohua Road 42#, Hefei, Anhui 230029, China. Tel.: +86 551 6360 2031; fax: +86 551 6514 1078.
** Corresponding author at: CAS Key Laboratory of Materials for Energy Conversion, Department of Materials Science and Engineering, University of Science & Technology of China, Hefei, Anhui 230026, China. Tel.: +86 551 6360 2031; fax: +86 551 6514 1078.
E-mail addresses: suns@ustc.edu.cn (S. Sun), cgao@ustc.edu.cn (C. Gao).

http://dx.doi.org/10.1016/j.apcatb.2015.01.045
0926-3373/

the primary attacking species [27]. For example, Lin et al. [28] have found that partially isolated hydroxyl groups are more active than the others on P25 TiO_2, resulting in preferential consumption in the photocatalytic oxidation of toluene. Moreover, the sufficient hydroxyl groups from adsorbed water on TiO_2-coupled photocatalysts (e.g., TiO_2/SnO_2 and TiO_2/ZrO_2) favor the mineralization of toluene against the formation of partial oxidation products [18]. In other words, the hydroxyl groups on TiO_2 can serve as the most important adsorption sites and directly participate in photocatalytic degradation.

Therefore, many strategies focusing on the modification of the TiO_2 surface to optimize hydroxyl sites and in turn enhance the photocatalytic activity have been developed. Representative methods include the manipulation of surface roughness [25], incorporation of lanthanide ions [29], and hydration of nanostructured TiO_2 [19]. Recently, some studies have been devoted to optimizing the photocatalytic performance of TiO_2 by modifying the surface with different acidic or alkali species [30–35]. The modification of TiO_2 via sulfation has been proved to be an effective approach to enhance its degradation activity [30,31]. The main reason is that the surface sulfates on TiO_2 can preserve hydroxyl groups to a greater extent than pure TiO_2 [32]. However, the influence of the acidic or alkali species on the adsorption and photocatalytic activity of TiO_2 for air purification remains controversial. For example, the sulfur species possibly occupied some active adsorption sites, which in turn decreased the maximum adsorption capacity for contaminants [36]. Similarly, some studies have reported that the surface modification of TiO_2 with alkali species (such as NH_3) results in the decrease of UV-induced photocatalytic activity [37], which rectifies the promotion effect in some publications [33,34]. Besides, surface modification with acidic or alkali species can also lead to changes in the specific area, surface acidity, and behavior of photogenerated electron–hole pairs [38–40], which may complicate the nature of the photocatalytic process, and thus, this topic is worthy of investigation.

To comprehensively understand the above mentioned concerns, the adsorption and photocatalytic degradation of gaseous toluene on TiO_2 surface modified with H_2S and NH_3 species were investigated in this work. The influences of H_2S/NH_3 species on the adsorption of toluene on modified TiO_2 were presented. By in situ diffuse reflectance infrared Fourier transform spectroscopy (DRIFTS) equipped with a homemade reaction system and a coupling gas-dosing system, the adsorption mechanism and relationship between the surface structure and photocatalytic activity were also proposed.

2. Experimental

2.1. Preparation of photocatalysts

Pure TiO_2 powders were synthesized by a sol–gel method as described elsewhere [41]. The typical synthesis procedure was as follows. First, 10 mL of ethanol tetra-*n*-butyl titanate ($Ti(OC_4H_9)_4$, chemical pure) was dissolved in 16 mL ethanol (CH_3CH_2OH, chemical pure), and the precursor solution obtained was allowed to stir at room temperature. Next, the solution mixture containing 16 mL ethanol, 3.4 mL deionized water and 5.0 mL acetic acid (CH_3COOH, analytical pure) was added dropwise into the above precursor solution under vigorous stirring. The resulting transparent colloidal suspension was kept stirring for 30 min and then aged for 2 days till gel formed. The gel was dried at 353 K for 24 h, and then calcined at 753 K for 6 h in air to obtain pure TiO_2 powder. Hereafter, the obtained material will be designated as TiO_2–p. Acidic- and alkali-modified TiO_2 was obtained by treating the as-prepared pure TiO_2 in H_2S and NH_3 gas streams, respectively, at 423 K for 2 h (designated as TiO_2–H_2S and TiO_2–NH_3, respectively). The flow rate of the gas stream was adjusted to 10 sccm.

2.2. Characterization of photocatalysts

Powder X-ray diffraction (XRD) spectra were recorded on a Rigaku D/max-γA rotation anode diffractometer with Cu Kα radiation. X-ray photoelectron spectroscopy (XPS) measurements were conducted on a Thermo ESCALAB 250 XPS system with a monochromatized Al Kα X-ray source (1486.6 eV). All binding energies were referenced to the C 1s peak of surface adventitious carbon at 284.8 eV. The weight loss of these powders over a temperature range of 298–673 K was monitored by thermogravimetric analysis (TGA) in a thermobalance (TGA Q5000 V3.15 Build 263). Electron spin resonance (ESR) signals of the hydroxyl radicals and superoxide radicals spin trapped by 5,5-dimethyl-1-pyrroline-*N*-oxide (DMPO) in water and methanol, respectively, were recorded on a JES FA200 X-band spectrometer under irradiation with a 500 W Xe-arc lamp.

2.3. Photocatalytic activity

The activity of the samples for the photocatalytic degradation of gaseous toluene was investigated by a homemade setup (Fig. 1), which consists of a gas feed system, a photoreactor and an analytical system. The photocatalytic activity was tested using a 400 mL quartz photoreactor (Part I in Fig. 1). 0.2 g of the sample was first diffused into a certain amount of distilled water to form a suspension, followed by coating it on a glass substrate. Then it was dried at 323 K for 5 min and finally fixed at a suitable position in the photoreactor. The gaseous toluene and water vapor feed were obtained by bubbling 20 vol% O_2/N_2 compressed air through the saturators containing toluene and distilled water at 298 K, respectively. The light source employed for the photocatalytic reaction was a 300 W Xe-arc lamp (PLS-SXE300UV, Beijing Perfectlight Technology Co., Ltd.) equipped with an IR-cutoff filter for eliminating the thermal effect. The irradiation intensity at 365 nm on the photocatalyst surface was 215 mW/cm^2. Before the reaction, the sample was kept in the dark for 2 h to reach the adsorption/desorption equilibrium on the photocatalyst surface. The toluene concentration in the photoreactor was analyzed by a gas chromatograph (GC1690, Hangzhou Kexiao Scientific Instruments Co., Ltd.) equipped with a flame ionization detector (FID) and a chromatographic column (KX-112, Lanzhou Institute of Chemical Physics). The relative humidity (R.H.) in the photoreactor was determined using an electronic hygrometer. The initial toluene concentration was 500 ppmv, and the relative humidity level was R.H. 85%. The degradation rate of toluene was calculated by the equation of $(1 - C/C_0)\%$, where C_0 is the initial toluene concentration and C is the toluene concentration at intervals.

2.4. In situ DRIFTS

For in situ DRIFTS experiments, a Bruker IFS 66 v/s FTIR spectrometer equipped with a deuterated triglycine sulfate (DTGS) detector was used and operated under OPUS/IR software. A reaction system (Part II in Fig. 1), consisting of a praying mantis DRIFTS accessory (Harrick Scientific) and a reaction cell (HVC, Harrick Scientific) was employed. The reaction cell was equipped with a heater and housed a sample cup for the photocatalysts. A dome with three windows covered the sample cup and was maintained in place with retaining plates. Two of the IR transparent windows were made of KBr, while the third was made of quartz to allow the photocatalyst to be irradiated by UV light. The same light source used in the photocatalytic activity test was adopted for irradiation. In the experiment, the reactants entered and exited the cell through a set

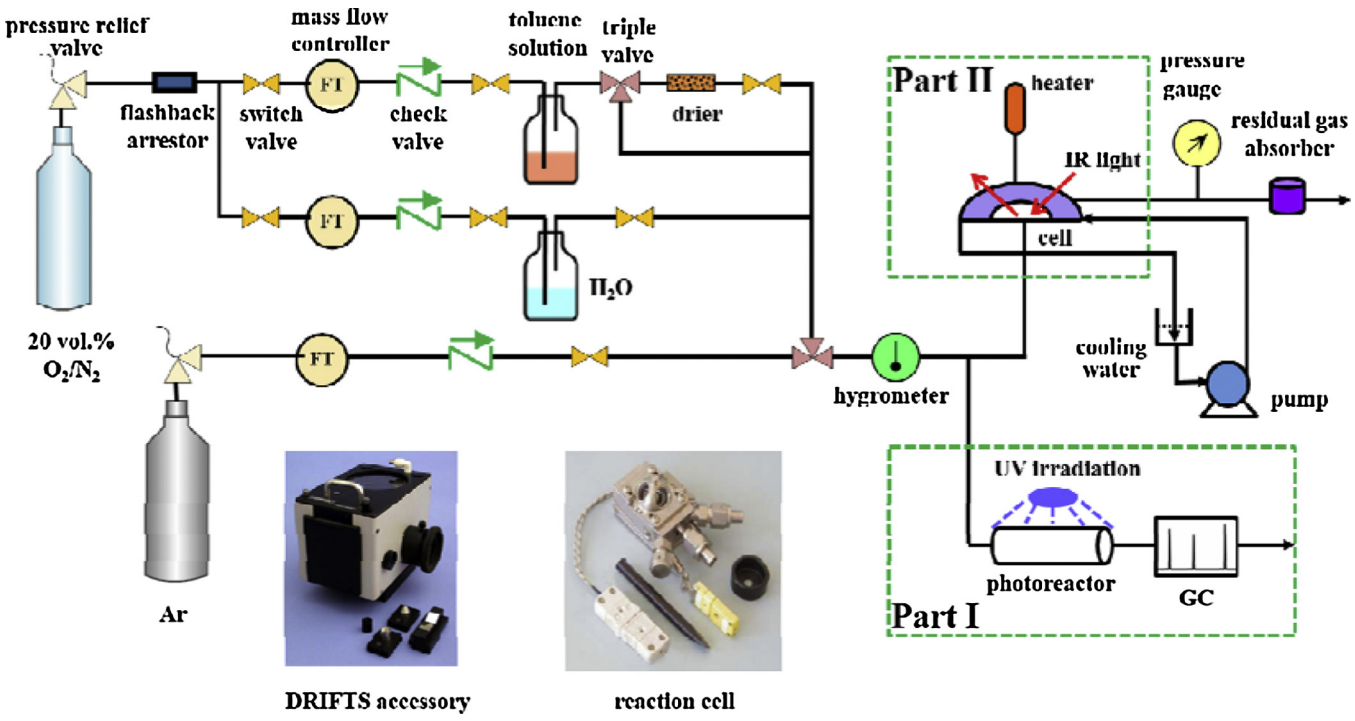

Fig. 1. Schematic diagram of the experimental setup for (Part I) the photocatalytic activity and (Part II) in situ DRIFTS measurements.

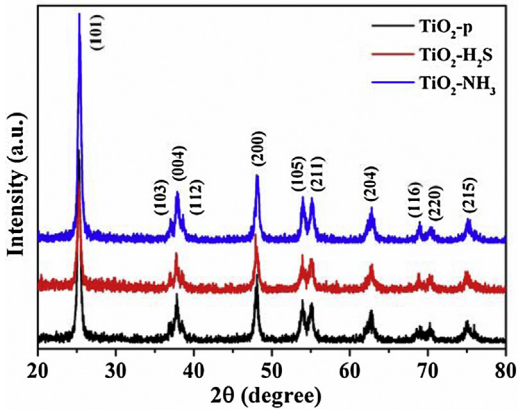

Fig. 2. XRD patterns of TiO_2–p, TiO_2–H_2S, and TiO_2–NH_3.

of inlet and outlet ports. The reaction gas flow rate was 10 sccm. The in situ DRIFTS spectra of toluene adsorption and photocatalytic degradation were collected in the range of 4000–600 cm^{-1} by averaging 40 scans with a resolution of 4 cm^{-1} at a scanning velocity of 10 kHz. A detailed account of the experimental setup has been reported elsewhere [36].

3. Results

3.1. Characterization of photocatalysts

Fig. 2 shows the XRD patterns of TiO_2–p, TiO_2–H_2S and TiO_2–NH_3 samples. For all the samples, the diffraction peaks at 2θ of 25.3°, 36.9°, 37.8°, 38.6°, 48.1°, 53.9°, 55.1°, 62.7°, 68.8°, 70.3°, and 75.0° can be indexed as the (1 0 1), (1 0 3), (0 0 4), (1 1 2), (2 0 0), (1 0 5), (2 1 1), (2 0 4), (1 1 6), (2 2 0), and (2 1 5) planes of anatase TiO_2 (JCPDS no. 21-1272), respectively [42]. No diffraction peaks corresponding to TiS_2 in the TiO_2–H_2S sample or TiN in the TiO_2–NH_3 sample were observed. The result indicates that in this study, the surface modification process by treating TiO_2 with H_2S and NH_3 gas at 423 K does not alter the crystalline phase of TiO_2 or cause ion incorporation in the TiO_2 lattice.

As shown in Fig. 3, XPS was employed to characterize the chemical states of O and Ti atoms in the samples. The intensities have been normalized to the same scale for ease of comparison. Two peaks of binding energy located at 529.8 ± 0.1 eV and 531.0 ± 0.1 eV, respectively, were observed in the O 1s core level spectra of all samples. The former peak was attributed to O^{2-} in the TiO_2 network, while the latter most likely corresponded to oxygen in the surface hydroxyl groups [43]. For the Ti 2p core level spectra, two peaks of binding energies located at 458.6 ± 0.1 eV and 464.4 ± 0.1 eV, respectively, were detected, corresponding to Ti $2p_{3/2}$ and Ti $2p_{1/2}$, respectively, suggesting that Ti^{4+} is the main component in all samples. As shown in Fig. 4, the chemical states of sulfur and nitrogen species in the as-prepared TiO_2–H_2S and TiO_2–NH_3 samples were also characterized. For TiO_2–H_2S (Fig. 4(a)), a peak was observed at 162.3 eV, corresponding to S^{2-} in the S 2p spectra. In addition, two peaks were observed at 169.2 eV and 167.9 eV, respectively, indicating that sulfur also had an oxidation state of +6 or +4 [44]. It means that a part of H_2S gas is present in the form of H_2S molecule on the TiO_2–H_2S surface, while the remaining H_2S might be oxidized by surface water [44]. For TiO_2–NH_3 (Fig. 4(b)), the N 1s core level spectra exhibited only one peak at 400.5 eV, suggesting that NH_3 is not oxidized and is mainly present in molecular form on the TiO_2–NH_3 surface [37]. It should be pointed out that it is hard to determine the concentration of H_2S or NH_3 contained in the TiO_2 surface layer accurately. However, the surface atomic ratios of S and N to Ti can be calculated semi-quantitatively to be 3.5% and 9.9%, respectively, from XPS results.

Fig. 5 shows the TGA curves of all samples. The total weight loss in the whole temperature range was 0.38% for TiO_2–p, 0.64% for TiO_2–H_2S and 0.47% for TiO_2–NH_3. In the case of TiO_2–p, the weight loss was ascribed to water desorption. In particular, the first region was below 408 K, over which the weight loss was 0.059%, caused by the loss of physically adsorbed water [45]. In the region of 408–673 K, the mass loss was approximately 0.32%, caused by the

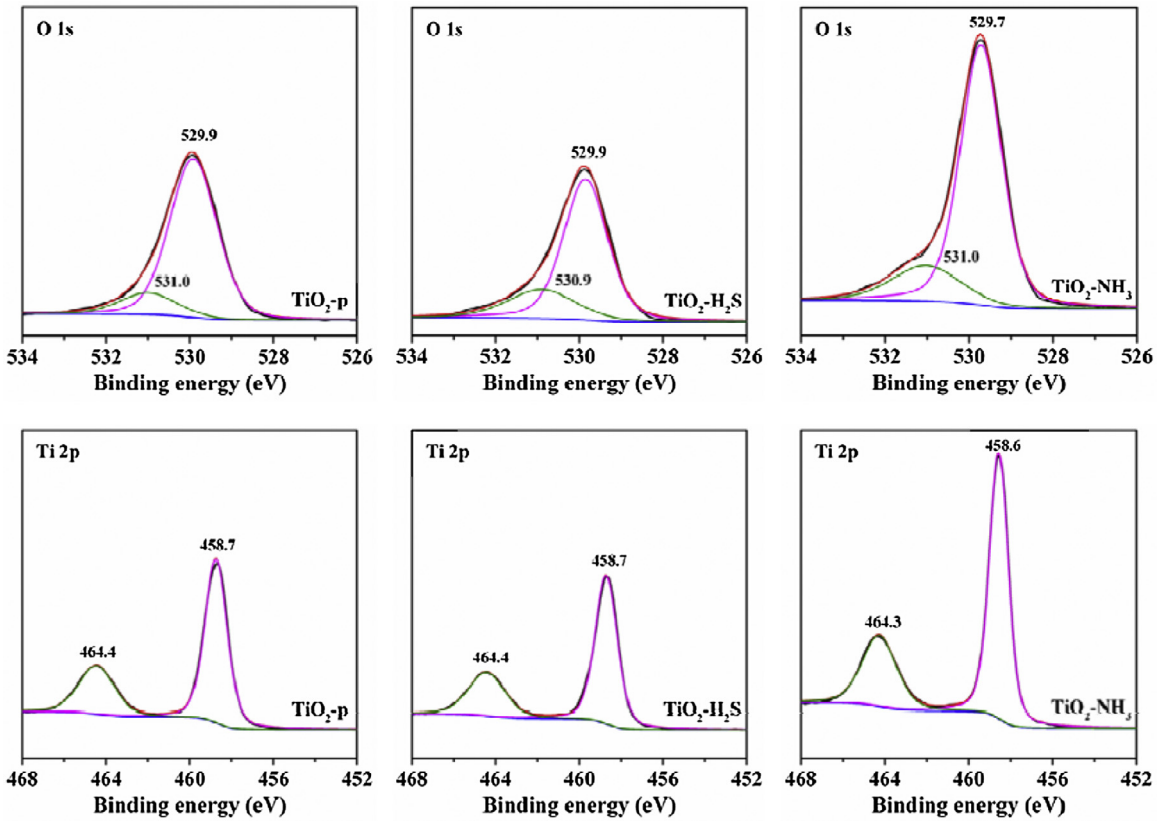

Fig. 3. XPS core level spectra of O 1s and Ti 2p for TiO_2–p, TiO_2–H_2S, and TiO_2–NH_3.

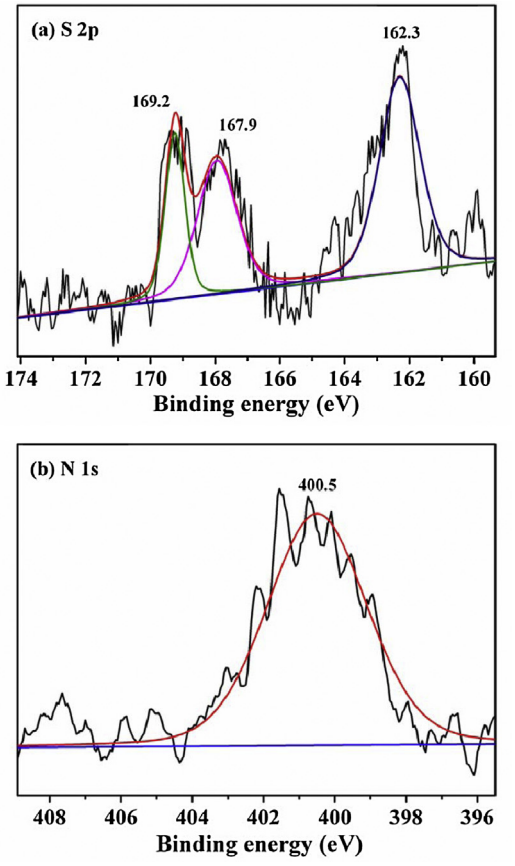

Fig. 4. XPS core level spectra of (a) S 2p for TiO_2–H_2S and (b) N 1s for TiO_2–NH_3.

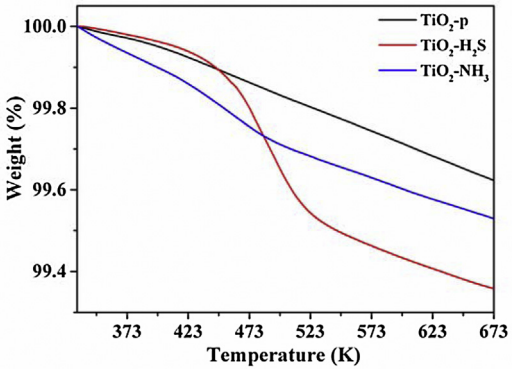

Fig. 5. TGA of TiO_2–p, TiO_2–H_2S, and TiO_2–NH_3.

removal of strongly bound water and surface hydroxyl groups [46]. For TiO_2–H_2S, three regions of weight loss were clearly observed. The first region was the same as that of TiO_2–p, which showed a 0.045% weight loss from room temperature to 408 K, corresponding to the loss of physically adsorbed water. In the region of 408–543 K, the mass loss was approximately 0.46% caused by the removal of adsorbed H_2S and strongly bound water or some surface hydroxyl groups. The third stage was from 543 to 673 K, where the mass loss can be attributed to the surface hydroxyl groups. Compared with the weight loss of TiO_2–H_2S, that of TiO_2–NH_3 exhibited insignificant features. In the whole region, the tendency of weight loss was similar to that of TiO_2–p. However, the weight loss was more than that observed in the case of TiO_2–p. It may be caused by the removal of the adsorbed NH_3 along with the removal of water and surface hydroxyl groups [47].

To compare the amount of active radicals in the samples during photocatalytic degradation, ESR spectra were recorded in the

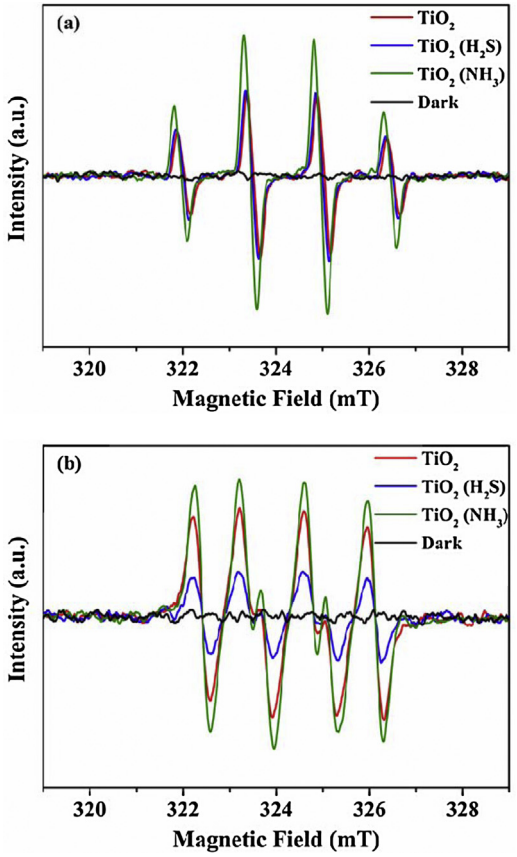

Fig. 6. DMPO spin-trapping ESR spectra for the (a) DMPO- $OH^{\bullet}$ and (b) DMPO- $O_2^{-\bullet}$ of TiO_2–p, TiO_2–H_2S, and TiO_2–NH_3 with UV irradiation.

same condition and shown in Fig. 6. In Fig. 6(a), a characteristic 1:2:2:1 quartet signal was observed, which indicated that $OH^{\bullet}$ radicals were generated during the photocatalytic reaction on all samples [48]. The signal intensity showed that the amount of $OH^{\bullet}$ radicals generated on the TiO_2–p and TiO_2–H_2S is almost equal and less than that on TiO_2–NH_3. The characteristic signals in Fig. 6(b) indicated that $O_2^{-\bullet}$ radicals are all generated during the photocatalytic reaction on the studied samples [49]. The amount of $O_2^{-\bullet}$ radicals was in the order of TiO_2–H_2S < TiO_2–p < TiO_2–NH_3.

3.2. Photocatalytic activity

The photocatalytic performances of the samples for toluene degradation with the initial concentration of 500 ppmv under R.H.

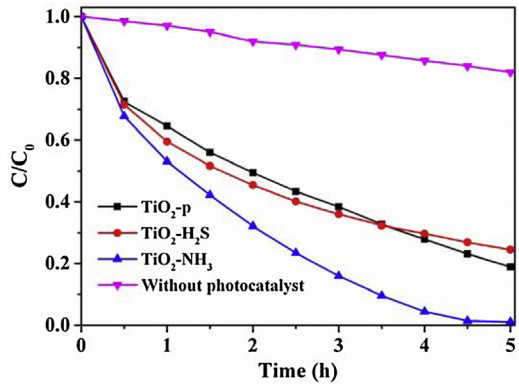

Fig. 7. Photocatalytic degradation activity of gaseous toluene on TiO_2–p, TiO_2–H_2S, and TiO_2–NH_3 photocatalysts.

85% were investigated and the results are shown in Fig. 7. The degradation of toluene under irradiation without photocatalyst, namely self-photolysis, was also performed under the same conditions for comparison. Only a small amount of toluene was self-photolyzed, indicating the as-synthesized samples are active for the photocatalytic degradation of toluene. Obviously, TiO_2–NH_3 exhibited a degradation rate (99%) significantly higher than those of TiO_2–p (81%) and TiO_2–H_2S (76%) in 5 h. In particular, the degradation on TiO_2–H_2S was faster than that on TiO_2–p in 3 h, however, the final degradation amount of toluene was smaller than that on TiO_2–p.

3.3. In situ DRIFTS results

Fig. 8 shows the DRIFTS spectra of the synthesized samples. The surface of fresh TiO_2 was relatively clean. The broad band in the range of 3400–2600 cm^{-1} can be attributed to the weakly bound water molecules and associated hydroxyl groups [19,39]. The band at 1624 cm^{-1} can be assigned to the bending mode (δ_{H-O-H}) of molecularly adsorbed water [19]. By contrast, a small band attributed to the bending vibration of δ_{H-S} was observed at 1439 cm^{-1}, suggesting the presence of sulfhydryl on the TiO_2–H_2S surface [50]. The modification of TiO_2 with NH_3 also introduced new bands for TiO_2–NH_3. The band at 1596 cm^{-1} can be attributed to the coordinated NH_3, while the bands at 1231 and 1166 cm^{-1} can be attributed to the symmetric deformation of NH_3 [51,52]. For investigating the trend of toluene adsorption on the photocatalysts surface, in situ DRIFTS tests were conducted. Fig. 9(a) shows the DRIFTS spectra of toluene adsorbed on TiO_2–p at room temperature. After toluene was introduced, new bands at 3074, 3035, 2940, and 2877 cm^{-1} appeared. The bands at 3074 and 3035 cm^{-1} were attributed to the ν_{C-H} of the aromatic ring, and 2940 and 2877 cm^{-1}

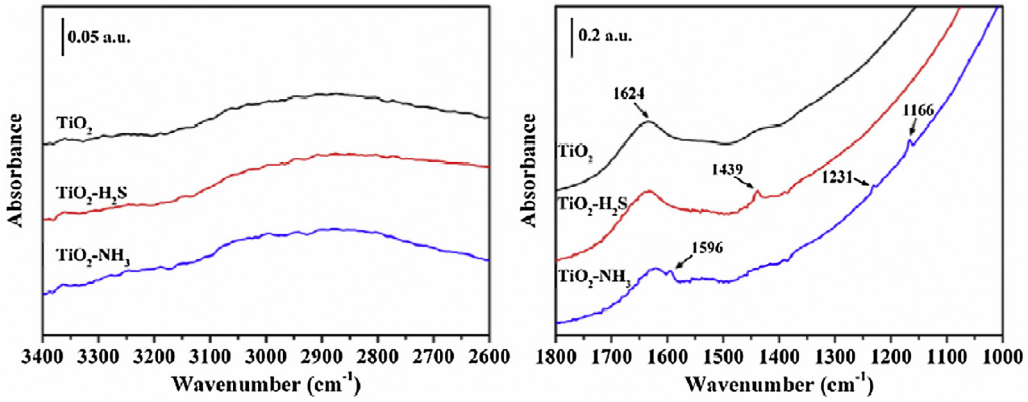

Fig. 8. DRIFTS spectra of TiO_2–p, TiO_2–H_2S, and TiO_2–NH_3.

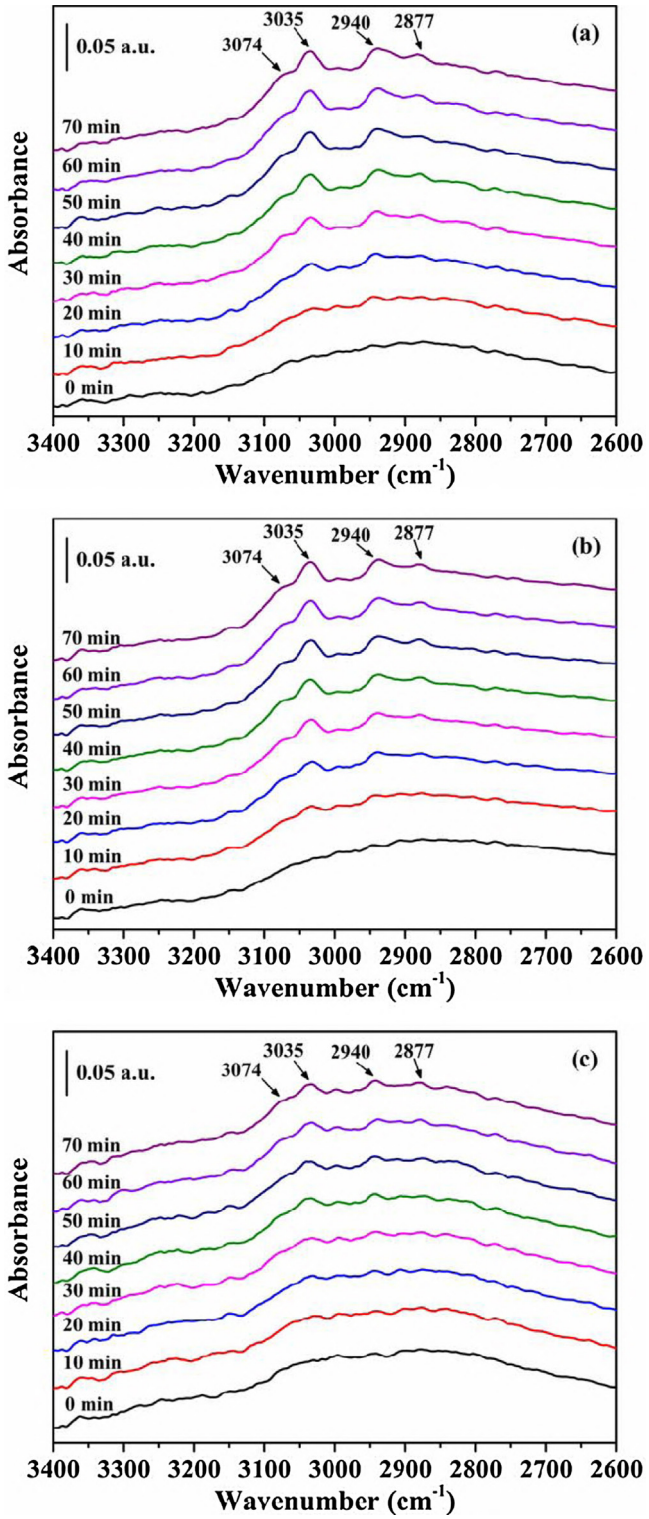

Fig. 9. In situ DRIFTS spectra of toluene adsorption on (a) TiO_2–p, (b) TiO_2–H_2S, and (c) TiO_2–NH_3 photocatalysts.

were assigned to asymmetric and symmetric ν_{C-H} of the methyl group, respectively [19]. The intensity of these bands increased with time and gradually reached a stable level. Fig. 9(b) shows the DRIFTS spectra of toluene adsorbed on TiO_2–H_2S, which were very similar to those in Fig. 9(a). The same characteristic bands of toluene (3074, 3035, 2940 and 2877 cm^{-1}) were also observed and gradually reached a steady level. For TiO_2–NH_3 (Fig. 9(c)), although the characteristic bands of toluene appeared, the intensities of these bands were obviously weaker than those on TiO_2–H_2S and TiO_2–p after 70 min of adsorption, indicating that the adsorption capacity of TiO_2–NH_3 for toluene is smaller than those of TiO_2–p and TiO_2–H_2S.

After the adsorption of toluene reached a stable level, the samples were irradiated by UV light and the DRIFTS spectra are shown in Fig. 10. In the high wavenumber region, the characteristic bands of toluene decreased by different degrees for all the samples, indicating that adsorbed toluene was photocatalytically decomposed. In the low wavenumber region, many new bands appeared. The band at 1684 cm^{-1} was attributed to the carbonyl vibration of the aldehyde group, and the bands at 1560 and 1358 cm^{-1} may arise from the asymmetric and symmetric vibrations of COO^- group, respectively [53]. The small shoulder bands at 1649, 1604, 1540, 1495, 1454 and 1417 cm^{-1} were attributed to various vibrations of the aromatic ring, and methyl and carboxyl groups. These characteristic bands were almost identical with those of pure TiO_2 treated with benzaldehyde and benzoic acid in the study of Cao et al. [13] and those of our test over Fe^{3+}–TiO_2 [41]. These results indicated that the intermediates, such as benzaldehyde and benzoic acid are formed and adsorbed on the photocatalyst surface. It clearly showed that there were significantly more intermediates on TiO_2–H_2S because the corresponding bands on TiO_2–H_2S were significantly strengthened in comparison to TiO_2–p.

4. Discussion

4.1. Effect of surface modification with H_2S/NH_3 on TiO_2 for toluene adsorption

In situ DRIFTS provides the real-time monitoring of transient events that are occurring on the photocatalyst surface during adsorption and photocatalytic reaction. For the ease of understanding, the intensity of the characteristic ν_{C-H} peak (3035 cm^{-1}) for toluene as a function of the adsorption time on TiO_2–p, TiO_2–H_2S and TiO_2–NH_3 is shown in Fig. 11. From the plots, these three photocatalysts clearly differed in their adsorption capacity. The toluene was adsorbed more rapidly on TiO_2–H_2S than on TiO_2–p and TiO_2–NH_3, especially at the beginning of the adsorption process. The adsorption capacity of toluene on TiO_2–NH_3 was significantly smaller than those of toluene on the other two samples. Of note, the surface areas of the samples were similar (Supporting information, Section 1) because they were synthesized by the same thermal treatment. Therefore, the difference in the adsorption of toluene between these samples in this study cannot be attributed to the surface areas. Fig. 12 shows the adsorption kinetic profiles of toluene on the three samples, in which two types of kinetics model: zero-order kinetics model and Langmuir–Hinshelwood (L–H) model, were used to fit the experimental results. In the figure, I stands for the intensity of the characteristic band at 3035 cm^{-1} and I_t is the balanced intensity shown in Fig. 9. The adsorption of toluene on the three photocatalysts was probably a two-step process. For TiO_2–p, TiO_2–H_2S and TiO_2–NH_3, in the first 25 min, 22 min and 17 min, respectively, the experimental data were observed to be in good agreement with the zero-order model with apparent rate constants of 5.6×10^{-4}, 9.8×10^{-4} and 3.3×10^{-4}, which were estimated according to the slope of the fitting line (inset of Fig. 12). In the second-step process, the adsorption of toluene on the three photocatalysts was a typical L–H model of the first-order reaction with rate constants of 0.020, 0.014, and 0.028 for TiO_2–p, TiO_2–H_2S, and TiO_2–NH_3, respectively.

In the case of naked TiO_2 exposed to water vapor, the surface can be hydroxylated as a result of the dissociative chemisorption of molecular water to satisfy the co-ordination of surface Ti^{4+} sites [27]. The dissociation of water on the TiO_2 surface forms two

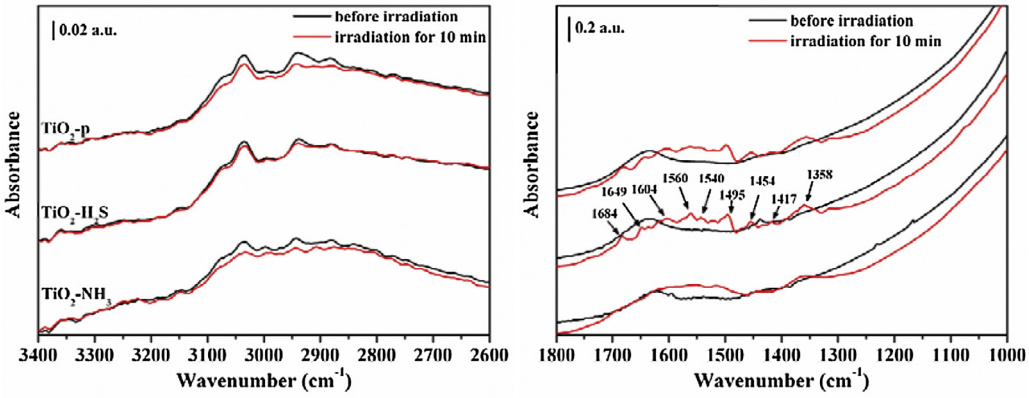

Fig. 10. In situ DRIFTS spectra of toluene oxidation on (a) TiO_2–p, (b) TiO_2–H_2S, and (c) TiO_2–NH_3 photocatalysts with UV irradiation.

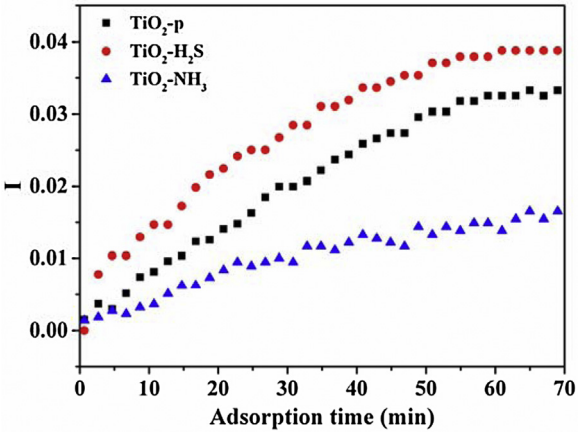

Fig. 11. Plots of the intensity of the characteristic ν_{C-H} peak (3035 cm^{-1}) for toluene versus adsorption time for the TiO_2–p, TiO_2–H_2S and TiO_2–NH_3 photocatalysts.

distinctive hydroxyl groups: one hydroxyl group bridges two surface vicinal Ti^{4+}, while the other forms a terminal Ti—OH group [16,54]. As known, the surface hydroxyl groups acting as active adsorption sites are crucial to the adsorption of toluene on the TiO_2 surface because toluene is suggested to be adsorbed on TiO_2 via an OH···π-electron-type interaction [11,21]. For TiO_2–H_2S, H_2S molecules and sulfhydryl groups were present on the TiO_2–H_2S surface, which is demonstrated by the XPS (Fig. 4(a)) and DRIFTS (Fig. 8) results. Therefore, it is reasonable to believe that H_2S molecules on TiO_2 surface are also dissociated to satisfy the co-ordination of the surface Ti^{4+} sites [55]. The formed types of sulfhydryl group are doubly-coordinated sulfhydryl groups and singly-coordinated sulfhydryl groups, respectively, as shown in Scheme 1. It can be inferred that sulfhydryl groups are the active sites on TiO_2–H_2S surface for toluene adsorption and that the toluene can be adsorbed on the sulfhydryl groups through an SH···π-electron-type weak interaction similar to that with hydroxyl groups on pure TiO_2. It may be easier to adsorb toluene on sulfhydryl groups as against on hydroxyl groups, resulting in a higher adsorption rate on the TiO_2–H_2S surface than on TiO_2–p at the start of adsorption process, which was reflected by DRIFTS (Fig. 9) and semi-quantitative results (Fig. 11). It should be pointed out that, according to TGA (Fig. 5) and DRIFTS results (Supporting information, Section 2), some hydroxyl groups still existed on the TiO_2–H_2S surface, since the competitive dissociative chemisorption of molecular water and H_2S occurred during the modification process. In fact, according to the desorption results reported in literature [19,20], the OH···π-bonded aromatic ring is more stable even under outgassing for several minutes. Our desorption experiments also proved that (Supporting information, Section 3). Therefore, the OH···π-electron-type interaction may be stronger than the interaction of toluene with surface sulfhydryl species. That is, the OH···π-electron-type interaction is significantly stronger, but the SH···π-electron-type is favorable for the adsorption of toluene. As a result, when introducing toluene onto the TiO_2–H_2S surface, the adsorptive capacity and adsorption rate for toluene increased in comparison to pure TiO_2.

The NH_3 interaction with TiO_2 was quite different. Previous studies have documented that NH_3 is less likely to be adsorbed dissociatively on the empty sites in the presence of water [56]. In this study, the TGA result of the TiO_2–NH_3 and DRIFTS spectra of hydroxyl groups on the samples before the adsorption of toluene (Supporting information, Section 2) have revealed that lots of physically adsorbed water and surface hydroxyl groups exist on the TiO_2–NH_3 surface. In Combination with XPS (Fig. 4(b)) and DRIFTS (Fig. 8) results, which show that surface nitrogen species are present in the form of NH_3 molecules on TiO_2–NH_3, it indicates that NH_3 adsorbs on Ti^{4+} sites or hydroxyl groups without dissociation. In the first instance, as known, Ti^{4+} is a stronger Lewis acid center and NH_3 is a strongly basic molecule, thus NH_3 molecules can be strongly adsorbed on Ti^{4+} through direct H_3N···Ti bonding, as shown in Scheme 2(a). In this case, toluene can interact with coordinated NH_3 by an HN···π-electron-type interaction on the TiO_2–NH_3 surface. Furthermore, NH_3 coordinated on Ti^{4+} results in the weakening of the acidity of surface hydroxyl groups, which weakens the interaction of toluene with hydroxyl groups [57]. It is in agreement with the DRIFTS results (Fig. 9), in which the existence of NH_3 negatively affects the toluene adsorption. In the latter instance (Scheme 2(b)), NH_3 modification promotes NH_3 adsorption on hydroxyl groups since the TiO_2 surface is hydroxylated and large portions of Ti^{4+} are occupied by hydroxyl groups. Notably, the doubly coordinated hydroxyl group is more acidic than the singly coordinated hydroxyl group. Hence, NH_3 adsorbs more strongly on a bridging hydroxyl group than on a terminal hydroxyl group [56]. However, the steric hindrance probably interferes the interaction of toluene with NH_3 or hydroxyl groups, which was also observed by DRIFTS. As a result, the modification of TiO_2 with NH_3 inhibits the adsorption of toluene to some extent. To support the understanding of the surface structure, the density of states of the samples was investigated by theoretical simulations (Supporting information, Section 4). Briefly, electron delocalization was weakened on TiO_2–NH_3 and resulted in the reduction of the adsorption ability, which also agreed with the analyses above.

4.2. Effect of surface modification with H_2S/NH_3 on TiO_2 for toluene degradation

In general, gas–solid heterogeneous photocatalysis is surface-sensitive, and the surface physical and chemical properties of

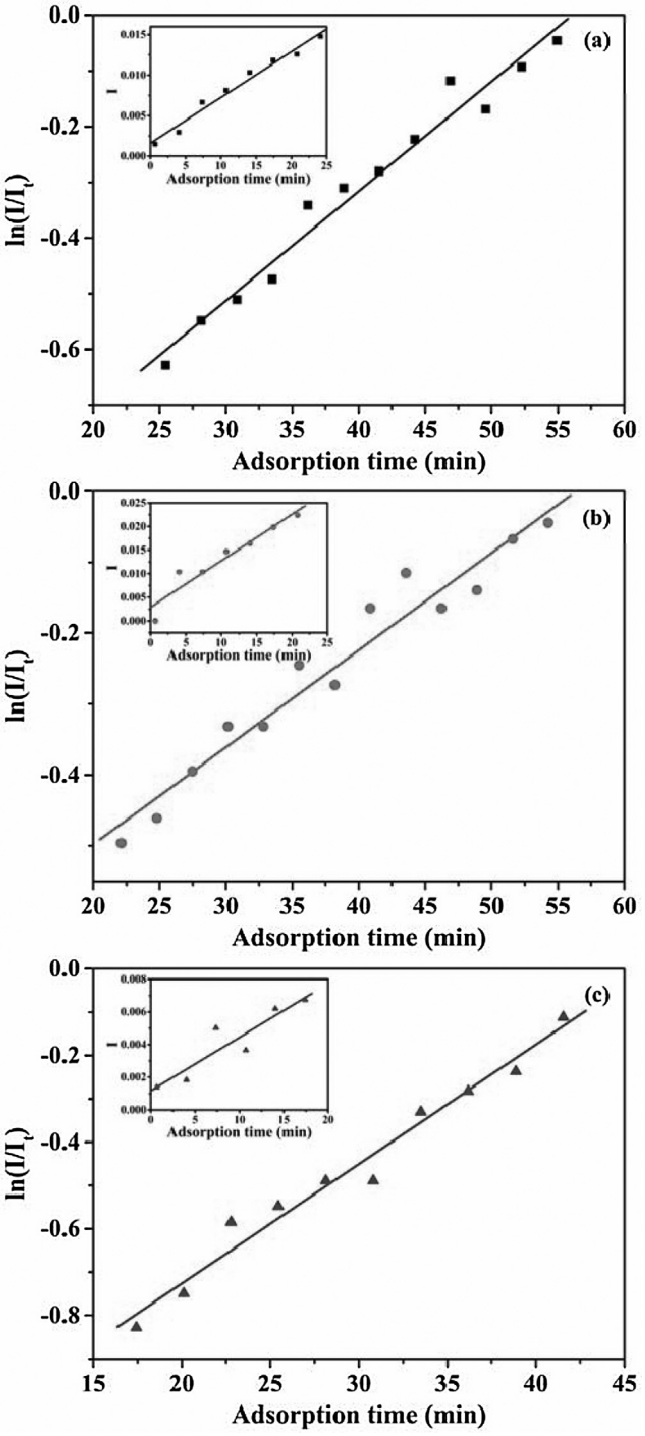

Fig. 12. Kinetics plots for toluene adsorption on (a) TiO_2–p, (b) TiO_2–H_2S, and (c) TiO_2–NH_3 photocatalysts. Insets represent the zero-order model in the former 25 min (TiO_2–p), 22 min (TiO_2–H_2S), and 17 min (TiO_2–NH_3).

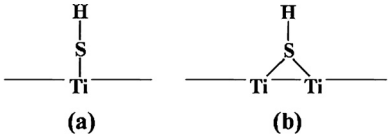

Scheme 1. Schematic surface structure of TiO_2–H_2S.

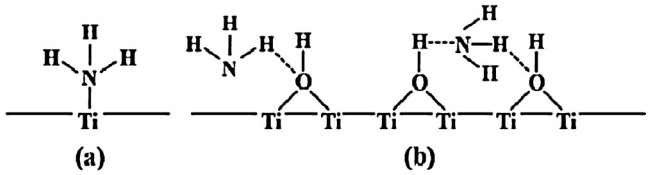

Scheme 2. Schematic surface structure of TiO_2–NH_3.

a photocatalyst can affect the reaction processes. In this study, significant differences in the photocatalytic performance of the as-synthesized samples were revealed by comparing toluene adsorption and degradation. It implies that the relevant surface modification of TiO_2 determines the differences among these photocatalysts. It should be pointed out that these photocatalysts show similar optical properties (Supporting information, Section 5). Therefore, the difference in the photocatalytic activity between these samples in this study is not attributed to the light absorption. Although TiO_2–NH_3 has been proven to exhibit the lowest adsorption capacity for toluene, it exhibited the highest photocatalytic activity for the degradation of toluene. One of the main reasons is that NH_3 modification preserves lots of physically adsorbed water and surface hydroxyl groups on the TiO_2–NH_3 surface, which was determined by the DRIFTS spectra of hydroxyl groups before and after toluene adsorption (Supporting information, Section 2). The adsorbed water molecules and hydroxyl groups are the most abundant electron donors which can react with photogenerated holes to produce $OH^{\bullet}$ radicals [58]. $OH^{\bullet}$ radicals are an extremely powerful and indiscriminate oxidant and can rapidly attack pollutants on the surface [59]. Moreover, the photogenerated electrons are free to react with the adsorbed oxygen to produce a reactive superoxide radical ($O_2^{-\bullet}$) [60,61]. The ESR study exactly proved that TiO_2–NH_3 generates more $OH^{\bullet}$ and $O_2^{-\bullet}$ radicals than TiO_2–H_2S and TiO_2–p. In addition, the oxidation of NH_3 with O_2 can lead to the formation of nitrates during the photocatalytic process which may promote the photocatalytic activity [51].

For TiO_2–H_2S, its photocatalytic performance for the degradation of toluene is very interesting. The degradation rate of toluene on TiO_2–H_2S was faster at the start of degradation, but the final degradation amount of toluene was smaller than that on TiO_2–p. Generally, the photocatalytic activity depends on the adsorption ability, quantum efficiency of the photo-generation of the electron–hole pairs, and separation of the electron–hole pairs, among others [8]. Most important of all, TiO_2–H_2S exhibited the highest adsorption capacity for toluene. Secondly, during the photocatalytic process, the surface sulfur species were oxidized by O_2 or superoxide radical ($O_2^{-\bullet}$) to form SO_4^{2-} which are more likely to preserve surface hydroxyl groups to a greater extent than on TiO_2–p [32]. Besides, the positive effect of sulfates at the initial degradation stage can also be attributed to their high capacity to capture photogenerated electrons, thus lowering the recombination of the electron–hole pairs [26,39]. This observation is in agreement with literature [62]. The subsequent decrease of the degradation rate is due to the intermediate products, which cause photocatalyst poisoning. Many groups have devoted to identifying the intermediates, such as benzyl alcohol, benzaldehyde, and benzoic acid, and attributing the deactivation of the photocatalyst to the occupation of benzaldehyde and/or benzoic acid on the active sites on the photocatalyst surface [13,63,64]. In this study, the DRIFTS results indicate that benzaldehyde and benzoic acid are formed and adsorbed on the photocatalysts surface. The concentration of such compounds on the TiO_2–H_2S surface was higher than those on the TiO_2–NH_3 and TiO_2–p surface. The concentration of the intermediates in the gas phase detected by gas chromatography (Supporting information, Section 6) also confirmed the above mentioned result. However, the amount of $O_2^{-\bullet}$ radicals generated from

TiO_2–H_2S is obviously less than those from TiO_2–NH_3 and TiO_2–p (ESR results in Fig. 6(b)). Therefore, it can be concluded that the intermediates cannot be effectively oxidized by the relatively small amount of $O_2^{-\bullet}$ radicals. Besides, significantly more sulfates were formed as the reaction proceeded in a closed environment, which may be detrimental to the rehydroxylation [65], thereby further decreasing the degradation rate after reaction for 3 h. Last but not least, as documented in the literature [66], the byproducts formed in the photocatalytic oxidation of H_2S may likely be another reason to lead to the deactivation of photocatalyst. It must be noted that in some studies [67,68], the higher the bonding energy of the adsorption, the better the degradation efficiency. However, this is not consistent with the results in this study. It may be due to the differences between the surface properties, adsorption structure, and target pollutants.

5. Conclusions

The effects of pretreatment with H_2S and NH_3 on TiO_2 respectively for the adsorption and photocatalytic degradation of toluene were investigated. It was found that the surface modification with H_2S causes the dissociative adsorption of H_2S on the TiO_2 surface to satisfy the co-ordination of the surface Ti^{4+} sites. The formed sulfhydryl groups are favorable for toluene adsorption by the interaction of the aromatic ring with sulfhydryl groups. The surface sulfates positively affect the preservation of surface hydroxyl groups and the separation of photogenerated electron–hole pairs but may negatively affect the regeneration of the surface hydroxyl groups. At the start of the reaction, the high adsorption ability and inhibition ability of the recombination of electron–hole pairs of surface sulfates dominate the photocatalytic process and enhance the degradation rate. By contrast, in the latter part of the reaction, the inhibition of the regeneration of surface hydroxyl groups and poor generation of $O_2^{-\bullet}$ radicals lead to the accumulation of the highly stable intermediates, thus lowering the degradation efficiency. In the case of NH_3 modification, NH_3 is strongly adsorbed on Ti^{4+} through a direct $H_3N\cdots Ti$ bonding or adsorbed on the surface hydroxyl groups. Steric hindrance interferes the interaction of toluene with NH_3 or hydroxyl groups, thus decreasing the adsorption of toluene. The large amount of the adsorbed water molecules and hydroxyl groups on the surface might lead to the fact that TiO_2–NH_3 exhibits a good photocatalytic activity.

Acknowledgements

This work was supported by National Basic Research Program of China (973 Program, 2012CB922004), National Nature Science Foundation of China (11205159, 11179034), and Anhui Provincial Natural Science Foundation (1308085MB27, 1408085MB25). The authors thank Dr. Yuyin Wang and Tao Shao for assistance on the DRIFTS measurements.

Appendix A. Supplementary data

Supplementary data associated with this article can be found, in the online version, at http://dx.doi.org/10.1016/j.apcatb.2015.01.045.

References

[1] W.B. Li, J.X. Wang, H. Gong, Catal. Today 148 (2009) 81–87.
[2] S. Wang, H.M. Ang, M.O. Tade, Environ. Int. 33 (2007) 694–705.
[3] R. Iranpour, H.H.J. Cox, M.A. Deshusses, E.D. Schroeder, Environ. Prog. 24 (2005) 254–267.
[4] W. Den, C.P. Huang, C.H. Li, Chemosphere 57 (2004) 697–709.
[5] H. Chen, C.E. Nanayakkara, V.H. Grassian, Chem. Rev. 112 (2012) 5919–5948.
[6] M.D. Hernández-Alonso, I. Tejedor-Tejedor, J.M. Coronado, M.A. Anderson, Appl. Catal. B 101 (2011) 283–293.
[7] A.J. Maira, K.L. Yeung, J. Soria, J.M. Coronado, C. Belver, C.Y. Lee, V. Augugliaro, Appl. Catal. B 29 (2001) 327–336.
[8] A. Mills, S.L. Hunte, J. Photochem. Photobiol. A 108 (1997) 1–35.
[9] N. Liu, C. Schneider, D. Freitag, U. Venkatesan, V.R. Marthala, M. Hartmann, B. Winter, E. Spiecker, A. Osvet, E.M. Zolnhofer, K. Meyer, T. Nakajima, X. Zhou, P. Schmuki, Angew. Chem. Int. Ed. 53 (2014) 1–6.
[10] X. Chen, L. Liu, P.Y. Yu, S.S. Mao, Science 331 (2011) 746–750.
[11] Y.A. Luo, W.S. Tai, H.O. Seo, K.D. Kim, M.J. Kim, N.K. Dey, Y.D. Kim, K.H. Choi, D.C. Lim, Catal. Lett. 138 (2010) 76–81.
[12] S.B. Kim, S.C. Hong, Appl. Catal. B 35 (2002) 305–315.
[13] L. Cao, Z. Gao, S.L. Suib, T.N. Obee, S.O. Hay, J.D. Freihauty, J. Catal. 196 (2000) 253–261.
[14] V. Augugliaro, S. Coluccia, V. Loddo, L. Marchese, G. Martra, L. Palmisano, M. Schiavello, Appl. Catal. B 20 (1999) 15–27.
[15] O. d'Hennezel, P. Pichat, D.F. Ollis, Photochem. Photobiol. A 118 (1998) 197–204.
[16] C.L. Bianchi, S. Gatto, C. Pirola, A. Naldoni, A. Di Michele, G. Cerrato, V. Crocella, V. Capucci, Appl. Catal. B 146 (2014) 123–130.
[17] X. Li, J.H. Ye, J. Phys. Chem. C 111 (2007) 13109–13116.
[18] F. Fresno, M.D. Hernandez-Alonso, D. Tudela, J.M. Coronado, J. Soria, Appl. Catal. B 84 (2008) 598–606.
[19] A.J. Maira, J.M. Coronado, V. Augugliaro, K.L. Yeung, J.C. Conesa, J. Soria, J. Catal. 202 (2001) 413–420.
[20] P. Davit, G. Martra, S. Coluccia, J. Jpn. Petrol. Inst. 47 (2004) 359–376.
[21] M. Nagao, Y. Suda, Langmuir 5 (1989) 42–47.
[22] F. Zhang, X.D. Zhu, J.J. Ding, Z.M. Qi, M.J. Wang, S. Sun, J. Bao, C. Gao, Catal. Lett. 144 (2014) 995–1000.
[23] E. Farfan-Arribas, R.J. Madix, J. Phys. Chem. B 107 (2003) 3225–3233.
[24] K.I. Hadjiivanov, D.G. Klissurski, Chem. Soc. Rev. 25 (1996) 61–69.
[25] K.L. Yeung, S.T. Yau, A.J. Maira, J.M. Coronado, J. Soria, P.L. Yue, J. Catal. 219 (2003) 107–116.
[26] M.R. Hoffmann, S.T. Martin, W.Y. Choi, D.W. Bahnemann, Chem. Rev. 95 (1995) 69–96.
[27] C.S. Turchi, D.F. Ollis, J. Catal. 122 (1990) 178–192.
[28] H.X. Lin, J.L. Long, Q. Gu, W.X. Zhang, R.S. Ruan, Z.H. Li, X.X. Wang, Phys. Chem. Chem. Phys. 14 (2012) 9468–9474.
[29] F.B. Li, X.Z. Li, C.H. Ao, S.C. Lee, M.F. Hou, Chemosphere 59 (2005) 787–800.
[30] S.K. Samantaray, P. Mohapatra, K. Parida, J. Mol. Catal. A: Chem. 198 (2003) 277–287.
[31] R. Gomez, T. Lopez, E. Ortis-Islas, J. Navarrete, E. Sanchez, F. Tzompanztzi, X. Bokhimi, J. Mol. Catal. A: Chem. 193 (2003) 217–226.
[32] F. Jiang, Z. Zheng, Z.Y. Xu, S.R. Zheng, Z.B. Guo, L.Q. Chen, J. Hazard. Mater. 134 (2006) 94–103.
[33] A. Sarkar, A. Shchukarev, A.R. Leino, K. Kordas, J.P. Mikkola, P.O. Petrov, E.S. Tuchina, A.P. Popov, M.E. Darvin, M.C. Meinke, J. Lademann, V.V. Tuchin, Nanotechnology 23 (2012) 475711.
[34] J. Choina, D. Dolat, E. Kusiak, M. Janus, A.W. Morawski, Pol. J. Chem. Technol. 11 (2009) 1–6.
[35] O. d'Hennezel, D.F. Ollis, Helv. Chim. Acta. 84 (2001) 3511–3518.
[36] R.T. Yang, W.B. Li, N. Chen, Appl. Catal. A 169 (1998) 215–225.
[37] Z. Zhang, X. Wang, J. Long, Q. Gu, Z. Ding, X. Fu, J. Catal. 276 (2010) 201–214.
[38] H.M. Wu, J.Z. Ma, Y.B. Li, C.B. Zhang, H. He, Appl. Catal. B 152 (2014) 82–87.
[39] J.J. Murcia, M.C. Hidalgo, J.A. Navio, J. Arana, J.M. Dona-Rodriguez, Appl. Catal. B 142 (2013) 205–213.
[40] Y.X. Niu, M.Y. Xing, B.Z. Tian, J.L. Zhang, Appl. Catal. B 115 (2012) 253–260.
[41] S. Sun, J. Ding, J. Bao, C. Gao, Z. Qi, X. Yang, B. He, C. Li, Appl. Surf. Sci. 258 (2012) 5031–5037.
[42] C.Y. Song, W.J. Yu, B. Zhao, H.L. Zhang, C.J. Tang, K.Q. Sun, X.C. Wu, L. Dong, Y. Chen, Catal. Commun. 10 (2009) 650–654.
[43] Z. Zhang, J. Long, X. Xie, H. Zhuang, Y. Zhou, H. Lin, R. Yuan, W. Dai, Z. Ding, X. Wang, X. Fu, Appl. Catal. A 425–426 (2012) 117–124.
[44] V. Pore, M. Ritala, M. Leskela, S. Areva, M. Jarn, J. Jarnstrom, J. Mater. Chem. 17 (2007) 1361–1371.
[45] R. Mueller, H.K. Kammler, K. Wegner, S.E. Pratsinis, Langmuir 19 (2003) 160–165.
[46] K. Nagaveni, M.S. Hegde, N. Ravishankar, G.N. Subbanna, G. Madras, Langmuir 20 (2004) 2900–2907.
[47] F. Giraud, C. Geantet, N. Guilhaume, S. Loridant, S. Gros, L. Porcheron, M. Kanniche, D. Bianchi, J. Phys. Chem. C 118 (2014) 15677–15692.
[48] J.A. Rengifo-Herrera, K. Pierzchala, A. Sienkiewicz, L. Forro, J. Kiwi, C. Pulgarin, Appl. Catal. B 88 (2009) 398–406.
[49] J.Y. Li, W.H. Ma, C.C. Chen, J.C. Zhao, H.Y. Zhu, X.P. Gao, J. Mol. Catal. A: Chem. 261 (2007) 131–138.
[50] S. Kataoka, E. Lee, M.I. Tejedor-Tejedor, M.A. Anderson, Appl. Catal. B 61 (2005) 159–163.
[51] S.M. Lee, S.C. Hong, Appl. Catal. B 163 (2015) 30–39.
[52] R.B. Jin, Y. Liu, Y. Wang, W.L. Cen, Z.B. Wu, H.Q. Wang, X.L. Weng, Appl. Catal. B 148 (2014) 582–588.
[53] T. Chen, Z.H. Feng, G.P. Wu, J.Y. Shi, G.J. Ma, P.L. Ying, C. Li, J. Phys. Chem. C 111 (2007) 8005–8014.
[54] H.P. Boehm, Discuss. Faraday Soc. 52 (1971) 264–275.
[55] H. Zhang, X. Luo, H. Song, X. Lin, X. Lu, Y. Tang, Appl. Surf. Sci. 317 (2014) 511–516.
[56] A. Markovits, J. Ahdjoudj, C. Minot, Surf. Sci. 365 (1996) 649–661.

[57] K. Hadjiivanov, D. Klissurski, G. Busca, V. Lorenzelli, J. Chem. Soc. Faraday Trans. 87 (1991) 175–178.
[58] M.A. Henderson, Surf. Sci. Rep. 66 (2011) 185–297.
[59] R. Andreozzi, V. Caprio, A. Insola, R. Marotta, Catal. Today 53 (1999) 51–59.
[60] N. Quici, M.L. Vera, H. Choi, G.L. Puma, D.D. Dionysiou, M.I. Litter, H. Destaillats, Appl. Catal. B 95 (2010) 312–319.
[61] S.L. Lee, J. Scott, K. Chiang, R. Amal, J. Nanopart. Res. 11 (2009) 209–219.
[62] E. Barraud, F. Bosc, D. Edwards, N. Keller, V. Keller, J. Catal. 235 (2005) 318–326.
[63] J. Zhao, X. Yang, Build. Environ. 38 (2003) 645–654.
[64] R. Mendez-Roman, N. Cardona-Martinez, Catal. Today 40 (1998) 353–365.
[65] C. Xie, Z.L. Xu, Q.J. Yang, N. Li, D.F. Zhao, D.B. Wang, Y.G. Du, J. Mol. Catal. A: Chem. 217 (2004) 193–201.
[66] M.C. Canela, R.M. Alberici, W.F. Jardim, J. Photochem. Photobiol. A 112 (1998) 73–80.
[67] C.H. Ao, S.C. Lee, J.Z. Yu, J.H. Xu, Appl. Catal. B 54 (2004) 41–50.
[68] T. Noguchi, A. Fujishima, Environ. Sci. Technol. 32 (1998) 3831–3833.